Modern Geográfia
Vol. 18, Issue 2, 2023: 47–76
DOI: 10.15170/MG.2023.18.02.04

Gashi, Nazim[1] – Czigány, Szabolcs[2] – Pirkhoffer, Ervin[3] – Kiss, Kinga[4]

Modelling the Impact of Climate Change on the Flow Regime and Channel Planform Evolution of the Lower Drava River

ABSTRACT

Climate change is expected to have a significant impact on changing the flow regime of the lower Drava River. Four flume experiments were run to see how stabilized, increased and decreased flow and the occurrence of a series of floods affect channel planform evolution. Constant discharge produced alternate bars that subsequently merged into bigger bedforms, bedform migration, and a higher sinuosity of the channel. While merging and migration of bedforms may happen in the lower reaches of Drava, its sinuosity is unchanged due to river regulation. Reduced flow initiated transition from a braided to incised single-thread planform, with the formation of dormant channels. Drava already has a single-thread planform (because of dikes) and, in cases of flow reduction, will have the remnant of inactive channels. Increased discharge showed greater erosion and reworking of channel banks, a decrease of sinuosity ratio and active high bluff zones. On Drava sinuosity ratio is more difficult to change because of levees, but erosion, reworking of banks, and increased high bluff risks are possible. Floods simulation generated the construction of an anabranching planform alongside the incised main channel with terraces along banks (active during floods), bars, alluvial islands, and side channels (active during low flows). On the lower Drava River, this situation correlates with past floods.

Keywords: climate change, discharge, flume experiment, lower Drava River

1 MSc, GIS expert, UNICEF, Division of Data, Analytics, Planning and Monitoring, New York, USA, nazimgashi98@gmail.com
2 PhD, associate professor, head of the department, University of Pécs, Faculty of Sciences, Institute of Geography and Earth Sciences, Department of Physical and Environmental Geography, sczigany@gamma.ttk.pte.hu
3 PhD, associate professor, deputy head of institute, University of Pécs, Faculty of Sciences, Institute of Geography and Earth Sciences, Department of Physical and Environmental Geography, pirkhoff@gamma.ttk.pte.hu
4 PhD, assistant professor, University of Pécs, Faculty of Sciences, Institute of Geography and Earth Sciences, Department of Cartography and Geoinformatics, kissk@gamma.ttk.pte.hu

INTRODUCTION

The anthropogenic factor increasingly affects river channel patterns and morphology, as well as fluvial processes, landforms, and planforms (Debnath et al., 2015). Such control structures include dams, levees, and other flood-prevention structures, coastal protection and regulating systems, and changes in land use along the river. These changes in land use may have an impact on runoff conditions generating marked channel pattern changes. The use of physical models, such as flumes, that may adequately represent natural processes provides ideal tools to understand the intensity of these components (Kiss, 2021).

Despite the elimination of other elements that occur in actual rivers, flume experiments are valuable instruments for testing effects of erosion and deposition processes on river behavior (Słowik et al., 2021). Since the late 1800s, laboratory tests have been applied to model channel evolution. The earliest laboratory experiment of modeling meandering rivers took place in the 1930s (Tiffany & Nelson, 1939). The downscaled duplicate of the Mississippi River and its major tributaries (the Tennessee, Arkansas, and Missouri Rivers) on about 170 hectares, created in 1944 to help flood control planning and procedures along the river, is the biggest hydraulic model ever built (Foster, 1971). Leopold and Wolman (1957) used a constant discharge and sediment feed to replicate the development of a braided stream.

According to Schumm and Khan (1971), there is a strong link between the slope and sediment load concentration. With a low slope, river channels remain straight. On the other hand, a planform changes from straight to sinuous, then to a braided pattern, as the slope and sediment load increase. Schumm and Khan (1972) also found that when erosional and/or depositional thresholds are reached, channel patterns change swiftly (rather than gradually). They also determined that the presence of silts in sediments deposited to a riverbed contributes to the formation of meanders. Struiksma et al. (1985) used curved flumes with varying sinuosity and curvature radii to investigate changes in morphodynamics of bedforms and flow structure in meandering channels.

Previous research using flume tests aimed to simulate the influence of the vegetation on bank stabilization and meandering planform formation (Tal & Paola, 2007; Braudrick et al., 2009), and the influence of flow variability and the presence of fines on erosion prevention and bank stabilization (Métivier et al., 2016), and the creation of meandering rivers and cutoffs (e.g., Schumm & Khan, 1972; van Dijk et al., 2012, 2013; Li et al., 2019). Some other flume experiments were done by Słowik et al. (2021) to study how sediment starvation, flow deficit and the occurrence of a series of floods with sediment load influence the evolution of a channel planform.

The main goal of our study was to determine for the lower Drava River the impact of climate change-induced changes in discharge and flood occurrence on channel planform evolution.

The Drava River is a right-bank tributary of the Danube in southern Central Europe, flowing through the Dolomites at an elevation of 1,228 meters. The 725-km-long river forms a part of the Croatian–Hungarian border (166 out of 355 kilometers) in the Carpathian (Pannonian) Basin, and its

main tributary is the Mura River. The river has 22 hydroelectric power plants in Austria, Slovenia, and Croatia (Lóczy, 2019; Iskriva, n.d; Bali, 2008).

The Alpine section of the Drava-Mura catchment covers approximately 12,000 of the total 40,120 of the catchment. However, this section is responsible for two-thirds (ca 450 m^3 s^{-1}) of Drava's discharge (670 m^3 s^{-1}) at its confluence with Danube (Lóczy, 2019). Therefore, the current and future water regimes of the Drava and Mura Rivers are largely determined by the climatic conditions of the upland section (in Italy and mostly in Austria) (Blöschl et al., 2011; Baumgartner et al., 1983; Goler et al., 2016; Matulla et al., 2002).

In the Drava-Mura drainage basin, modeling approaches have also been used to forecast future climate conditions (Gobiet, 2010; Strauss et al., 2013). Downscaling regional climate models based on the A1B scenario, such as CLM (powered by the Global Climate Model ECHAM5), is an obvious option (Smiatek et al., 2009; Kromp-Kolb & Schwarzl, 2009; Schöner et al., 2011). The forecast is for the years 2021–2050, with 1976–2007 as a reference period. In comparison to the reference period, the average air temperature in Austria will rise by about 1°C, with summer warming being more pronounced.

Loss of biodiversity, ecosystem degradation, and climate change are all interconnected and have a serious impact on our socioeconomic stability, health, and well-being (Balatonyi et al., 2022). The physical environment is predicted to change as climatic conditions change (Lóczy, 2019). Observations in Osijek, Croatia, are being used to define climate change in the lower Drava basin (Cindrić et al., 2009). A positive winter temperature trend (+0.06 °C/10 years in Osijek) is typical for a continental region, according to one hundred years of observations. The decrease in yearly precipitation along the Drava River is due to lower rainfall levels in spring (Osijek: −4.1% in 10 years) and autumn (Osijek: −3.0% in 10 years) (Lóczy, 2019). From 1991 to 2020, the lowest discharge of the Drava River at the Drávaszabolcs station (the last Hungarian station) was during the winters of 2002 and 2012 with a discharge of 218 m^3/s and 234 m^3/s, respectively, in January.

Although the rate of change is modest, decade after decade, more and more precipitation quantities are observed in the Alpine sections of the Drava basin (Schmidli et al., 2002). In numerous Austrian research sites, Eitzinger et al. (2016) found that yearly precipitation was higher between 2002 and 2014 than the long-term (1981–2010) average.

Flood hazard along the Drava River is aggravated by snowmelt in the hilly Alpine foreland; followed by snowmelt in higher regions of mountains (conveyed through tributary river Mura) and Mediterranean cyclones causing a secondary peak in October or November (Lovász, 1972; Lovász, 1983). The discharge for 10 years of flood is about 2,100 m^3/s, while for 100 years of flood it is about 3,200 m^3/s (Lóczy, 2019).

The hydrological cycle is significantly affected by climate change (Schöner & Böhm, 2011; Goler et al., 2016). The Drava and its tributaries' early summer flood stages tend to decline, while water levels rise somewhat in autumn (Prettenthaler et al., 2007; Holzmann et al., 2010). Other earth systems, such as soil moisture (Kromp-Kolb & Schwarzl, 2009), geomorphological (Rickenmann, 2009)

and ecosystem processes, are also affected by climate change and even have serious socio-economic implications (Formayer et al., 2008).

The main consequence of hydroelectric power facilities and reservoirs is the disruption of sediment transport mechanisms, resulting in the river system being disconnected (Ristić et al., 2013). The disconnection is manifested in the form of flow regime alteration, a change in slope and velocity, which result in altered stream power conditions (Kiss & Andrási, 2011).

Over the period of 1991–2020, mean annual discharge at the Drávaszabolcs station ranged between 386 m^3/s (2003) and 781 m^3/s (2014), while the highest ever discharge for this period was measured on Sept. 19th, 2014 at 2220 m^3/s, and the lowest on Feb. 14th, 2002 at 167 m^3/s (South-Transdanubia Water Management Directorate, n.d.). Berényi et al. (2021) argue that in the Great Hungarian Plain there is a clear increase in the frequency and intensity of extreme precipitation events, in the length of dry periods, as well as in the occurrence of extreme weather events.

The main goal of our study was to determine the impact of climate change-induced changes in discharge and flood occurrence on channel planform evolution. Our research was based on flume tests, which allowed us to simulate the effects of alternating flows and channel incision on channel planform evolution. We also aimed at tracking the evolution of river planform in various flow and sediment delivery conditions, and comparing the results of flume experiments with the evolution of real river courses was among the research goals as well.

METHODS

Flume studies were conducted at the University of Pécs utilizing the PTETHYS (Project for Tectonical and Hydrological Simulations) flume (Figure 1). Both vertically and horizontally, the flume's push-blades may be adjusted. It may be tilted and adjusted along both its longitudinal (±7.5°) and transversal (up to 10°) axes. It includes six parts that can be moved vertically (±120 mm at 10–200 mm per day speed) and four push-blades that allow for 100 mm of lateral deformation. These adjustments can be applied to a variety of experiments, including tectonic and morphological processes. Computer-controlled electro-engines are in control of these movements. Only a sink in the downstream part of the flume allowed water and sediment to leave (Pirkhoffer et al., 2014; Słowik et al., 2021; Kiss, 2021).

The grain colors used in these experiments indicate grain size. Coarse grains are grey ground basalt (1 mm) and black andesite (0.8 mm). Red marble grains measuring 0.6 mm in diameter and beige limestone granules measuring 0.2 mm in diameter.

The flume is measured 4.4×2.3 m, with a maximum fill weight of 2,500 kg (wet sediment at a depth of 150 mm). A 1-meter-wide section of the entire flume was used for modeling purposes, with the bottom made of plexiglass. For the lateral constraints of flow, wooden boards were used. To prevent infiltration, the flume's surface was also secured with plexiglass. The discharge was measured and controlled by using a flow meter.

Sediment mobility in experiments may be low or below the threshold of motion when the discharge rate is decreased (Kleinhans et al., 2014). However, this can be partially overcome and compensated with higher slopes to increase the mobility of coarser sediment (Peakall et al., 1996; Kleinhans, 2010). Another solution can be to increase discharge to pass the motion threshold. Therefore, for all flume experiments, the slope was 3°. This enabled sediment transport to begin, resulting in active morphodynamics and the development of river planforms. During the gradual change of input parameters (gradient, discharge and texture), phenomena typical of natural rivers were observed.

Images of actual planforms were taken every 60 seconds throughout the flume testing, using eight Canon EOS 1100D cameras (4 Samyang 16 mm f/2,2 and 4 Sigma 24 mm f/1,4 objectives) mounted on a system of cantilevers above the experimental area at a 30-cm distance from each other and a 1.2-m height above bed (Figure 2). Images were taken concurrently with each camera since the cameras were connected to a computer via USB connections. Pictures were obtained with an 80% horizontal overlap, enabling the 3D models of the planforms to be calculated. In the experiment, ten markers (ground control points, GCP) with known spatial coordinates were used as references. Coordinates of the GCPs were measured with a Sokkia total station (SET630RK3 D22897) in a local coordinate system. As a result, all 3D models obtained from four experiments were in the same coordinate system, allowing distance and volume measurements in the model space.

Figure 1. Images illustrating the main components of the PTETHYS flume's construction (Słowik, 2021).

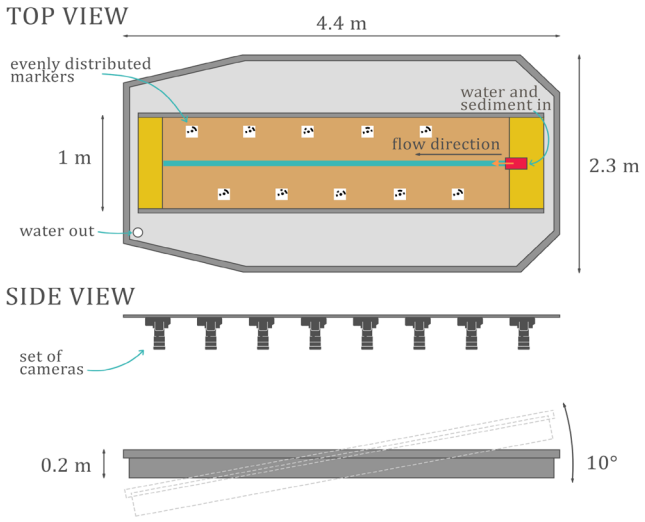

Photogrammetric methods

A photogrammetric range imaging technique called "*Structure from Motion*" (SfM) was used to estimate three-dimensional structures from sequences of two-dimensional images. Agisoft Metashape 1.8.0 was used to process the stereo pair images and render the topography.

Optically distorted images are created during image capture. To correct this and get an accurate model, we need to make a geometric correction and georeference the images. Geometric errors may be caused by several reasons, which may be related to the optical signal of the camera or surface.

The cameras are located at points on the field with a certain angle. This situation indicates the center of projection with three coordinates (x, y, and z), and direction can be given with three angles (ω, ϕ, and κ). These six values determine the exterior orientation parameters of the camera. In the case of perpendicular photography, ϕ and ω are close to 0. The errors caused by topographic relief mean that the heights of each point must be adjusted to the projection plane.

This method is also regularly applied in many studies on the field (Smith et al., 2016; Carrivick et al., 2016), by using drones or other vehicles.

Figure 2. Images depicting the PTHETHYS flume's construction: (A) View of the PTETHYS flume before installation; (B) The series of cameras installed for recording geomorphic processes; (C) A prepared flume prior to the start of an experiment

The availability of high-resolution models in geomorphological research is extremely important. The SfM was a good option for us since it is accurate, cheap, and fast. The SfM process is a complex set of algorithms that performs search for tie points and preparation of the point cloud. In the first step, it finds the same points on each angle (SIFT, ASIFT algorithm, Figure 3; Lowe, 2004).

The number of tie points (the same point from different angles) depends on the resolution of images and texture boundary of the assumed object, since if the texture is too homogeneous, it is more difficult to find the connection points.

After finding the tie points, a sparse point cloud is created (Figure 3A). After this step a dense point cloud is generated (Figure 3B). Then, an algorithm prepared the final model, i.e., a mesh surface model (Figure 3C). Once the mesh surface models were completed, the texture was built based on the generation of the ortophotos and DEMs (digital elevation models). Finally, the results as GeoTIFF files were exported.

Figure 3. Steps of SfM in Agisoft Metashape: (A) Sparse Point Cloud; (B) Dense Point Cloud; (C) Mesh Surface Model

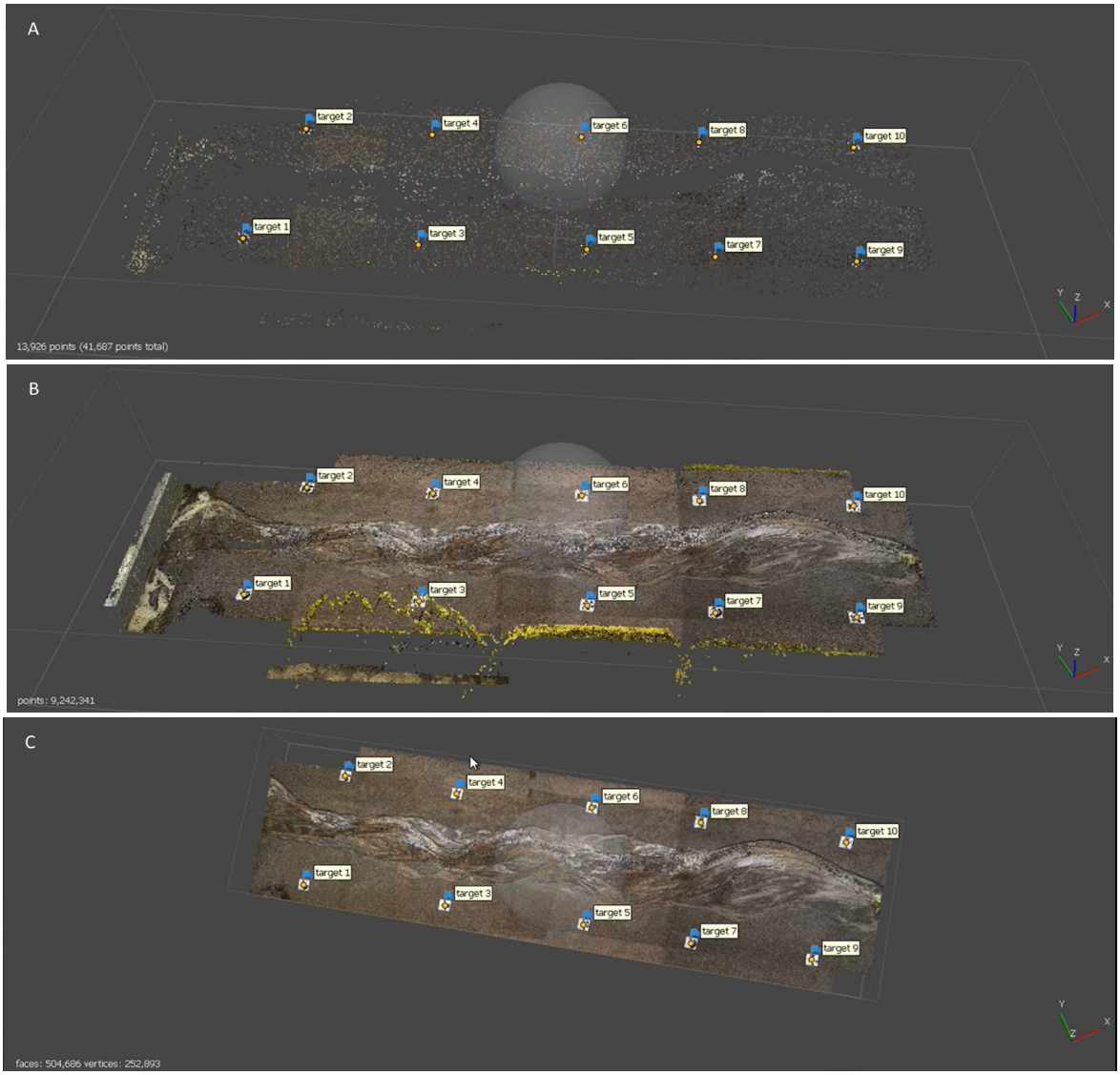

Methods of GIS processing

To obtain a detailed picture of the processes in the modeled riverbed, images were captured of the surface in 60-second time intervals. For the interpretation of digital elevation models and the detection of processes, ArcGIS Pro 10.8 (ESRI) was used.

Based on the obtained 3D models, channel planform changes were analyzed by cross-sectional profiles of channels and their immediate vicinity. Indices developed by several authors were utilized to determine channel patterns, to describe watercourses and to establish bed patterns.

For the channels created during the flume experiments, morphometric parameters were calculated: L_s: thalweg length; V: channel length; $\sum L_b$: total length of bars and islands; L_m: length of bars and islands on the given riverbed section. Furthermore, sinuosity (Leopold & Wolman, 1957; Rust, 1978) and braiding (Rust, 1978) indices were calculated (Table 1).

Table 1. Used morphometric measuring elements

	Author	Formula
Sinuosity	Leopold and Wolman 1957; Rust 1978	L_s / V
Braiding parameter	Rust 1978	$\sum L_b / L_m$

Setup of the flume experiments

From flume tests, three different variant tests about river discharge were run. The first test was on constant discharge magnitude, the second one on the decreased magnitude of discharge, and the third one on increased flow. Furthermore, another flume experiment was carried out simulating flood events when the flow was gradually increased. During all tests, the flume slope was constant (3°).

All flume tests began with a straight channel in a 2- to 6-cm-deep valley. The first 15 minutes were for the channel to advance to a state with active morphodynamics, in conditions of increasing or decreasing discharge. Therefore, a detailed analysis of the channel planform changes refers to a part of the conducted experiments. In the first experiment, changes of planform were shown from 60 minutes after the activation of the straight channel till the end of the experiment (120 min). For flume tests 2 and 3, experiments were analyzed for a period of 28 and 88 minutes. For the last experiment, analyses lasted for a period of 18 to 88 minutes, to compare the morphodynamics of floods.

Parameters of the experiments (Figure 4)

Test 1–simulation with constant discharge on planform evolution

Duration of experiment was 120 minutes, with 3 l/min discharge set to flow through a straight channel.

Test 2–simulation of decreased discharge on planform evolution

Duration of the experiment was 90 minutes, with 3 l/min discharge set to flow through a straight channel in the first 30 minutes of the test. Discharge was decreased to 2.5 l/min with a duration of 30 minutes and in the last 30 minutes of the experiment discharge was 2 l/min.

Test 3–simulation of increased discharge on planform evolution

Duration of experiment was 90 minutes. In the first 30 minutes of test, 3 l/min discharge was set to flow through a straight channel. Discharge was increased to 3.5 l/min for the next 30 minutes. And in the last 30 minutes of the experiment, discharge was increased again to 4 l/min.

Test 4–simulation of floods on planform evolution

Duration of experiment was 88 minutes, four cycles with 22 minutes each. In the first 20 minutes, discharge was 2 l/min, then in the following two minutes, discharge was 3.5 l/min. The cycle was repeated four times in the same channel without any interruption.

Figure 4. Setup of flume tests

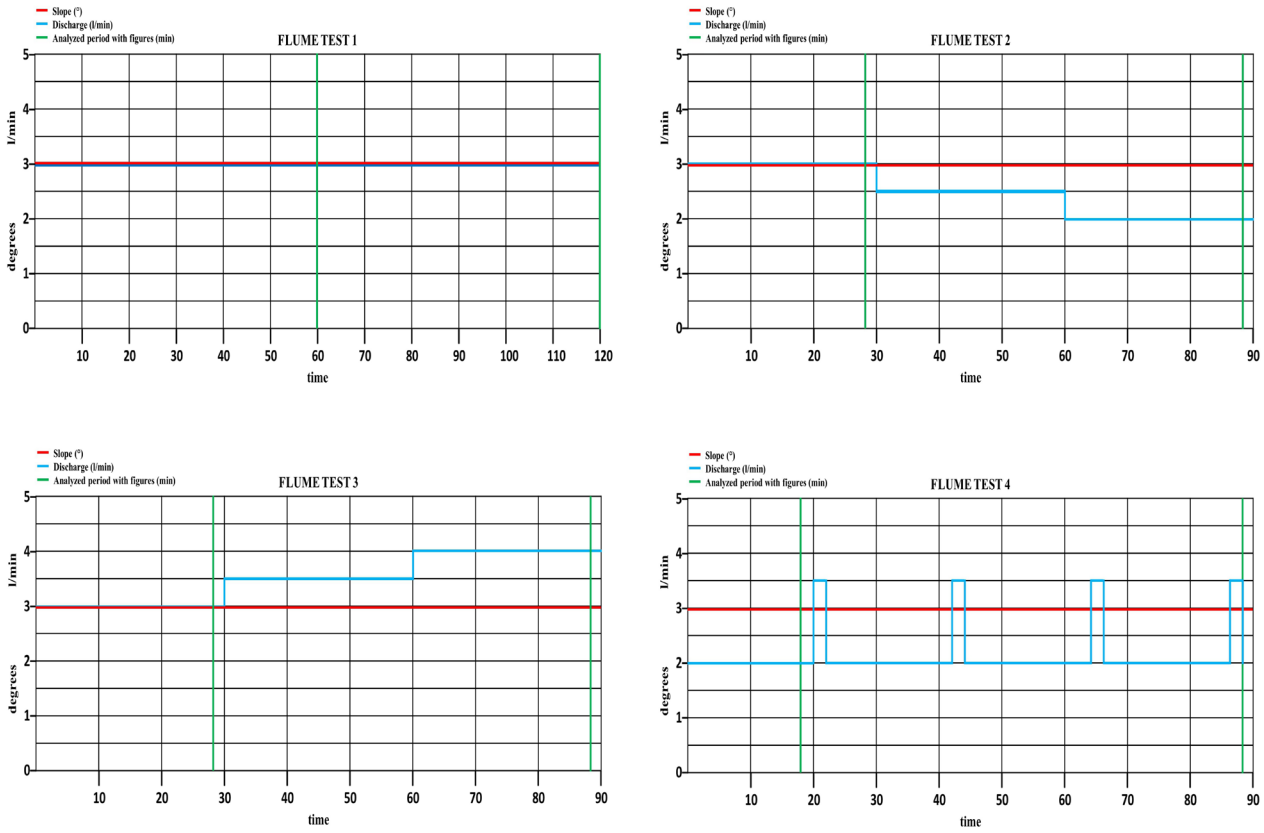

RESULTS

Channel Planform Evolution in Flume Test 1 (Figure 5)

The first experiment had a constant slope of 3°. The discharge, was also constant, with 3 l/min. From the initial straight channel, the riverbed evolved into a series of alternate bars, which can be named "free" bars. They were spontaneously developed because of the instability of the flow-bed system (Seminara & Tubino, 1989).

After 60 minutes of the experiment, the river started meandering, cut banks and bars of various lengths and sizes evolved throughout the channel. As water flowed across the flume, it eroded sediments and formed nearly vertical cut banks. Bars, due to the reduced flow and energy of water, were formed in the inner curve of the meanders' riverbed.

In the upper part of the river, meanders, bars, and cut banks were shorter in length compared to the middle and lower part of the river. For example, the average length of bars in the upper part (the first meter of flume) was 22 cm (min. 12 cm and max. 32 cm). In the middle part, the average length of bars was 22 cm too (min. 6 cm and max. 41 cm). In the lower part, the average bar-length was almost double compared to other parts (41 cm), while the minimum length was 15 cm and the maximum length was up to 60 cm. Furthermore, the channel planform was braided with some channels separating bars into smaller units.

With the exception of the increasing number of mid-channel bars in the middle reach, at the 120-minute mark of the experiment using constant discharge and slope, processes remained unchanged. Cut banks in the upper part were still under erosion with steep banks, while other cut banks in the middle and lower part were eroding at lower rates. In the lower part, the main flow was veered to the left side of the channel, while 60 minutes before the active channel had been flowing in the right corner of the bed. Now, the right corner was filled with bars.

Sinuosity ratio slightly decreased over the analyzed 120 minutes of the experiment. The braiding parameter, on the other hand, increased by the time the experiment reached 120 minutes. The area of bars stayed almost the same, while their number increased (Table 2).

Channel Planform Evolution in Flume Test 2 (Figure 6)

As in the previous test, the evolution of planform started with a straight channel, the downstream migration of alternate bars, and a sequence of side bars. The main channel began to meander, and bars began to build immediately (Figure 6). In the first 30 minutes of the test, with a discharge of 3 l/min, the flume consisted of multiple channels, separated by non-permanent bars (they were migrating downstream) formed within the channel. After 28 minutes in the experiment, in the upstream, terrace-like surfaces were built on the left side of the river. On the other hand, as the river was shifting to the right side, a cut bank (high bluffs) was created and as time moved on, the river was eroding more in that direction.

At an experimental time of 50 minutes, when the flow was decreased to 2.5 l/min, the river started to flow in the middle of the channel, and the cut bank was shifted to a lower position. Side bars were spread through the whole channel, but the largest of them was preserved in the upstream part of the flume, with no channel bars at all.

Almost an hour after the experiment began, the incision of the main channel was propagated upstream. In this manner, the side bars on either side of the main channel were raised above the level of the main channel and became inactive. A secondary channel of low flow appeared in the

middle part with some bars. As opposed to this, further downstream, an anabranching reach with an increased number of bars (compared to 30 minutes before) appeared.

Figure 5. The channel planform evolution at constant discharge (flume test 1): (A) Meandering river with active high bluffs on the main channel; (B) Alternate bars that subsequently merged into bigger bedforms and migrated downstream

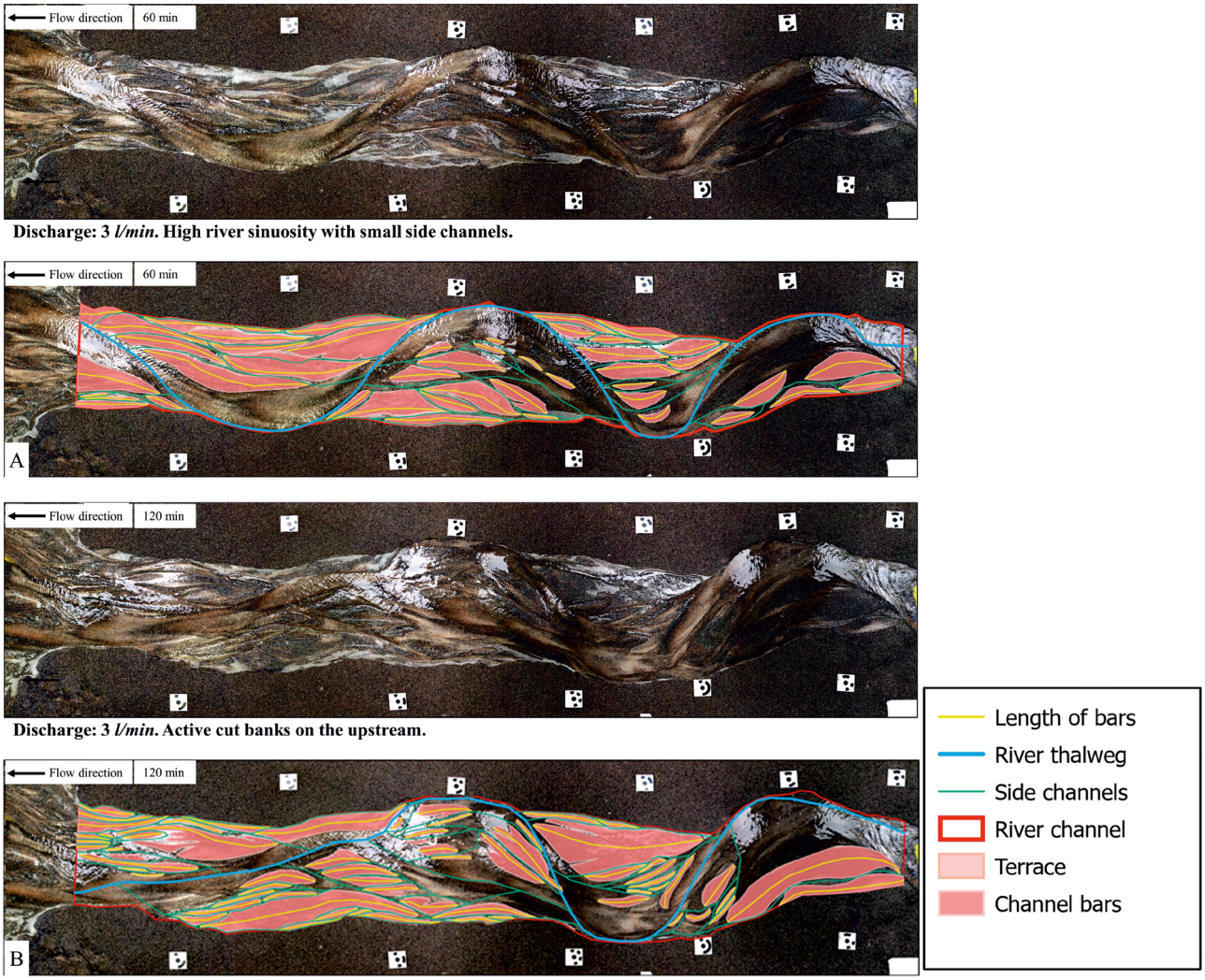

After further decrease of the flow to 2 l/min, at the 80-minute mark of the test, flow direction slightly changed (Figure 6). Bifurcation appeared upstream on the right side of the floodplain, and at 80 minutes of the test, this new stream became the main channel. The former main channel now was only a secondary channel with low flow. Between these two channels, alluvial islands were formed. The cut bank, which was active for more than an hour, now was part of the secondary channel, therefore not a lot of erosion was going on there. The number of bars in flume decreased, but their size increased. In the calculation done for this flume test, sinuosity ratio from 28 minutes to 88 minutes of experimental time gradually decreased. On the other hand, the braiding parameter, the area of bars, terraces, and alluvial islands increased (Table 2).

Figure 6. The channel planform evolution at the decreasing discharge (flume test 2): (A) An anabranching planform with active high bluffs; (B) A braided planform with an incised single-thread planform; (C) weak flow on the planform with sediment transportation and other morphological changes

Cross-sections of Flume Test 2

In the cross-sections, planforms captured at different times are shown (Figure 7). Starting from the first one, where the stream was on the right and the terrace on the left side of the channel. At 58 minutes, the main channel was in the middle with terraces on both sides. By end of the experiment, terraces remained on both sides, channel bars in the middle and a side channel on the left.

At the second cross-section, after 28 minutes of the experiment, the river was flowing in the entire width of the channel with active bluffs on both sides. Thirty minutes later the river was directed on the right side and on the left side a huge terrace was created with inactive side channels on it. At 88 minutes, the river flow was diverted to the center with two different flows, which had an alluvial island in the middle and terraces on both sides.

The main channel at the third cross-section (28 min) was a bit on the left with a secondary channel on the right side, which was separated from the main channel with a lateral channel bar. Terraces were present on both sides, being higher on the right side but wider on the left one. At 58 minutes, similarly to the previous cross-sections, an incised single-thread channel was observed, with terraces on both sides. Thirty minutes later (88 min) the main channel was wider but shallower with terraces on both sides and inactive side channels on the left side, except for one of them, which was still active.

At the last cross-section the downstream river was anabranching (28 min) with a lateral channel bar in the center and terraces on both sides. Terraces on the right were markedly higher than on the left. After decreasing the flow, at the 58th minute of the experiment, the flow slightly veered to the left with an additional side channel on the right (Figure 7). Thirty minutes later (88 min) we had a braided planform with several side channels in this region (only two at this cross-section).

Channel Planform Evolution in Flume Test 3 (Figure 8)

With a constant slope of 3° and at a discharge of 3 l/min, the flow was gradually increased every 30 minutes by 0.5 l/min. Under these circumstances, the riverbed changed from a straight channel, through the formation of a sequence of alternate bars, to a sequence of side bars (Figure 8).

After 28 minutes of the experiment, the river was lightly meandering a bit, and in the upper part, cut banks were more expressed due to the erosion on the right bank, while side bars were concentrated on the left in various shapes and sizes. A secondary channel was also formed here, with less water than in the main channel. Further downstream, the river followed a straighter line and bars were spread on both sides of the river. When we compare bars from here to the upper part, bars in the lower part have higher lengths and are bigger in size.

After 30 minutes, when the flow was increased to 3.5 l/min, at the 58th minute of the experiment, a huge side bar was created on the upper right side of the river. The river created an even more curved meander, but the water flowed in multiple channels. The secondary channel, visible in the first analyzed image, was still active. In addition, other channels were created in the lower reaches. As a direct consequence of the increased discharge, the number of bars increased, whereas their size decreased.

Figure 7. Cross-sections showing the evolution of the channel planform during the flume experiment 2. Check the figure above for the location of cross-sections
Ch: Channel; T: Terrace; B: Bar; R: Reflection; SCh: Side Channel

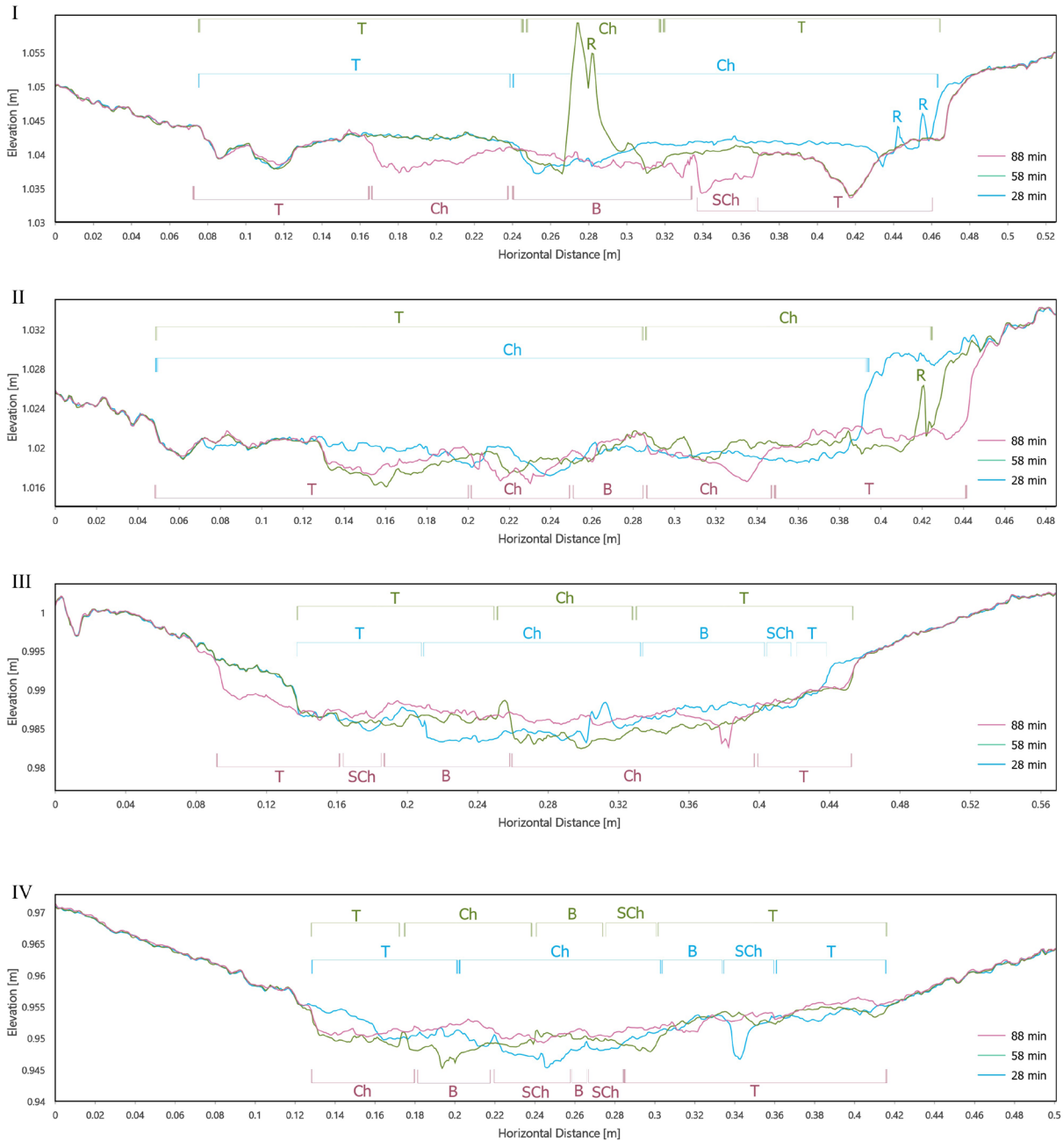

After a further increase of the flow to 4 l/min, the flow was conveyed through different channels. Still, the main channel was the one with even more curved meanders. The river had even smaller bars (with decreasing size) and was branching more. Due to the interaction between internal sinuosity thresholds and the flow enhancement, at this stage of the experiment meander cutoffs occurred. Some sections of the river diverted from the main stream of the watercourse and rejoined the main channel downstream. In the lower left part of the river, from the second analyzed image, a secondary channel was observed. Now, this channel had the highest discharge. The former main channel in this part

now was only part of river branches, while the dimensions of the side bars increased in all directions (Figure 8). The sinuosity ratio during flume test 3 increased over the period of 28 to 88 minutes (while at flume test 2 it decreased). The braiding parameter and the area of bars, terraces and alluvial islands increased as well (Table 2).

Cross-sections of Flume Test 3

From the third flume test, the cross-sections below were analyzed for research purposes. The main channel at the first cross-section at the beginning (28 min) was located on the right side of the river, while later it shifted to the left (58, 88 min). At the 28th minute of the experiment, close to the first cross-section an area was observable with many side channels and channel bars (Figure 9). At 58 minutes, a channel was formed on the left and a terrace on the right, whereas 30 minutes later the river shifted further to the left with a secondary channel of low flow.

At cross-section II the river had a main channel with a terrace on the left, which was part of the erosion from meandering. The situation changed a bit at the 58th minute, when the river followed two different paths dissected by a point bar. At 88 minutes of the experiment, discharge was 4 l/min and the river started meandering. The main channel of the river shifted to the right with active bluffs of high relief. To the left from the main channel, bars were formed and side channels were activated.

At the third cross-section, 28 minutes after the start of the flume test, the main channel had neither terraces nor channel bars. However, 30 minutes later, the channel extended to both sides and a channel bar was created on the right. After increasing the discharge again, at 88 minutes, the river began meandering to the left (a continuation of the preliminary meander from the second cross-section) and channel bars, side channels, and terraces were formed on the right.

At the final cross-section downstream, at the 28th minute of the experiment, a single-thread channel emerged with terraces on both sides. After increasing the discharge by 0.5 liter per minutes, at 58 minutes, the main channel concentrated on the right side, while side channels and channel bars were observable on the left (Figure 9).

Channel Planform Evolution in Flume Test 4 (Figure 11)

The slope was 3˚, while discharge at the start was 2 l/min. During the first 20 minutes, the planform evolved from straight to a braided planform with mid-channel bars migrating downstream. In the upper part, bars were inundated during flood events. The flow started out over the entire width of the channel, and the channel was widened, especially in the lower part (Figure 11). Before the flood, the channel was narrower and had fewer bars (mid-channel and alternate bars), while after the flood, the channel size increased by 12%, the number of bars increased and they were concentrated in the middle and lower part. This continued in other stimulated floods as well. Side bars before the flood were wider, while during the flood they were narrowed.

Figure 8. The channel planform evolution at the increasing discharge (flume test 3): (A) A braided planform with terraces on the left side; (B) After 58 minutes of the experiment, higher sinuosity ratio with smaller channel bars; (C) Even higher sinuosity ratio with active high bluffs.

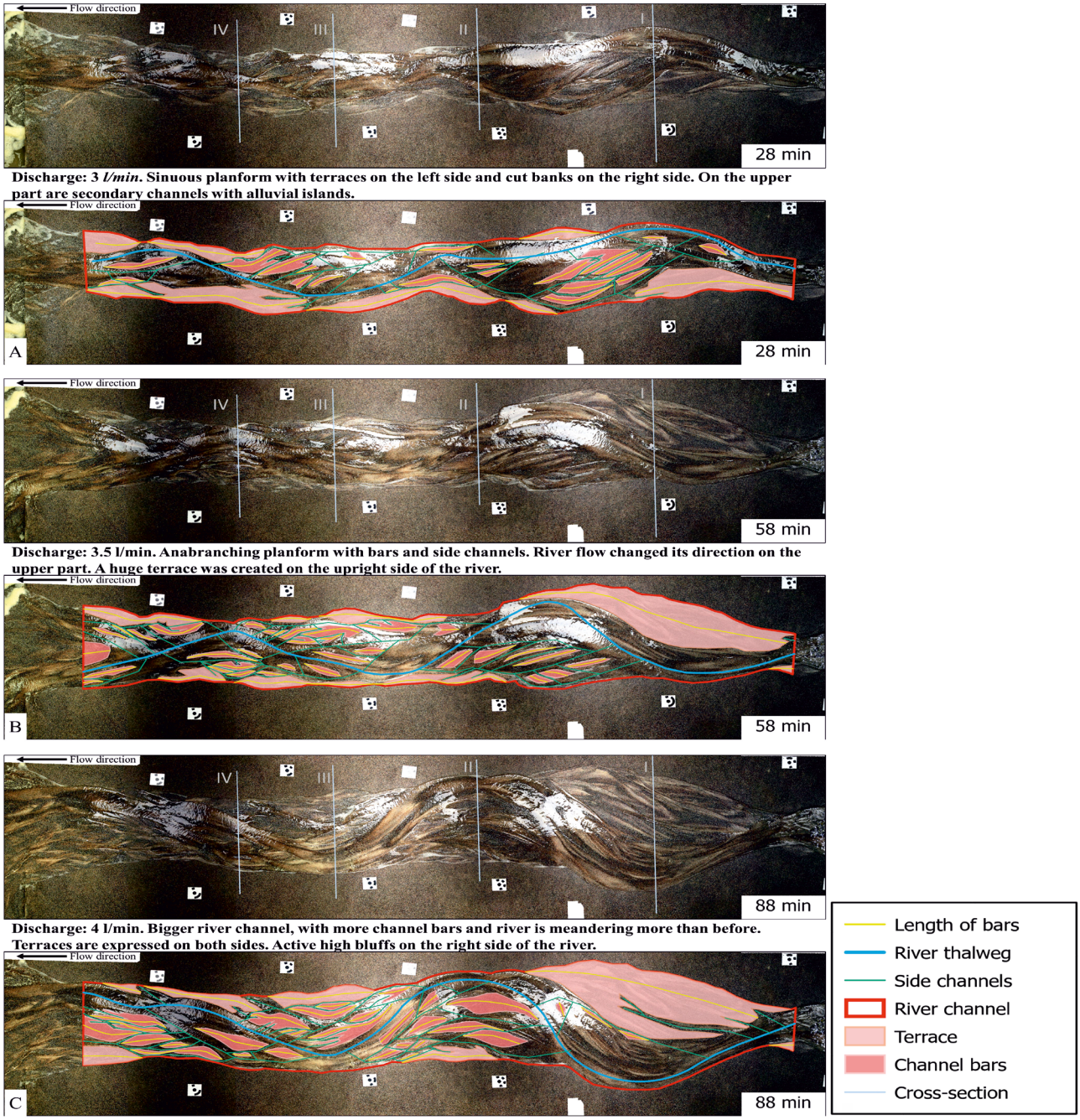

During the second flood, mid-channel bars were inundated, while side bars were reactivated, as being part of the main channel. The sediments of the side bars in the upper part were transported to the downstream and helped in the creation of a lot of bars. As a result, we had an anabranching planform.

Almost the same situation was observed during the next simulated flood event. The surface area of the bars was reduced. The area of the side bars and the channel bars was reduced by 50 and 12%,

respectively. During the flood, a cut bank was active in the upper right side of the river. The main channel continuously widened during the simulated flood.

Figure 9. Cross-sections showing the evolution of the channel planform during flume experiment 3.
Check Figure 8 for the location of the cross-sections
Ch: Channel; T: Terrace; B: Bar; R: Reflection; SCh: Side Channel

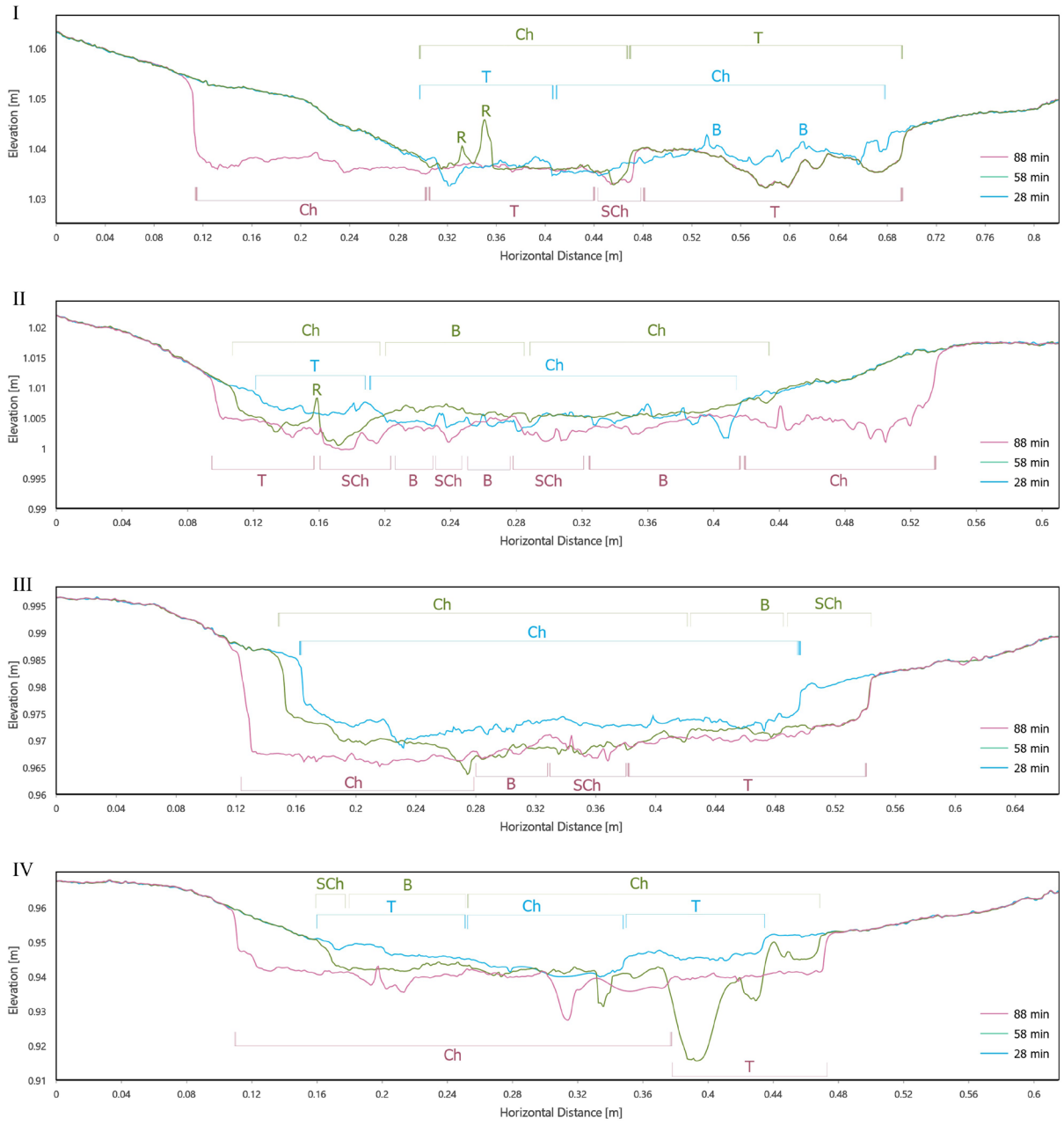

The series of simulated floods led to a successive rise in bar surfaces (Figure 10). During floods, the bars were reshaped or flooded, whereas during periods of low flows, the area of bars increased due to conveying the flow by the incised main channel. The number of bars and their area had cyclical dynamics (except in the first cycle the number of bars did not decrease, but the area did). During low flows, the number of bars was higher than during the flood periods. The same finding was shown

in the area of bars and alluvial islands. Overall, the total area of bars increased over this simulation period (see Table 2).

Figure 10. Surface changes and bar numbers during every cycle of the high and low flow on flume test 4.

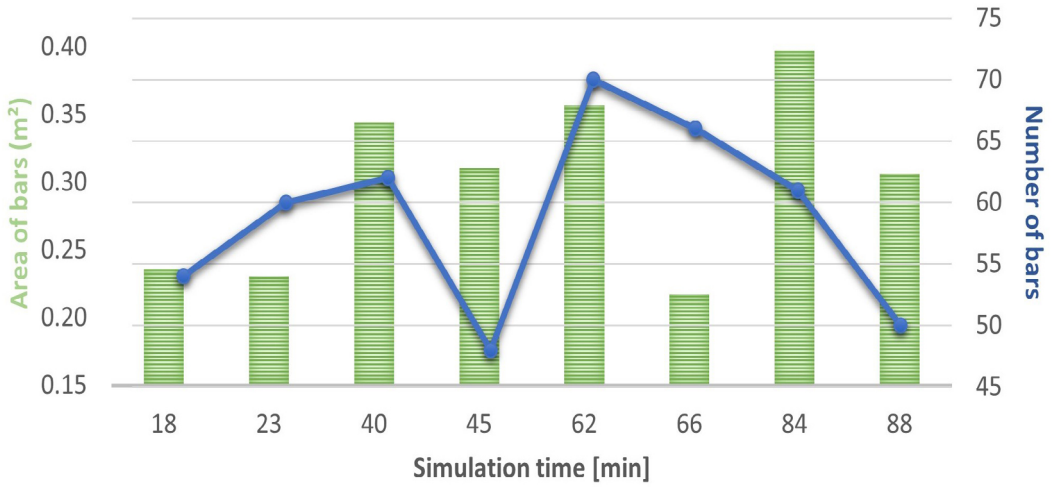

Because of the increased channel bar surface after floods, one main channel and several side channels, which were active at high flows, the obtained channel planform can be defined as anabranching.

Cross-sections of the Flume Test 4

From the fourth flume test, eight cross-sections are presented (Figure 12 and Figure 13) and the first four will be elaborated on (Figure 12) for every cycle of the floods generated on the flume test.

From the first cycle of the flood, we have cross-section II (see Figure 11 to understand the location of the second cross-section of the first cycle of the flood). During low flow, there was a single-thread channel with terraces on both sides, which had a higher altitude. After the first flood at 23 minutes, channel width was the same but the terrace on the left was missing because of inundation. A reflection is shown on the graph below, indicated by the letter R, which was caused by the water surface.

From the second flood the fourth cross-section was analyzed (see Figure 11 for cross-section location). Before the flood (2 l/min, 40 min), the main channel was on the right side of the river with an active secondary channel, a channel bar on the left and terraces on both sides. During the flood with 3.5 l/min, the main channel was on the right side, with some active and inactive side channels, channel bars on the left, and terraces on both sides.

From the third cycle of the flood, cross-section II was analyzed (see Figure 11 for cross-section location). At the 62-minute mark of the experiment, just before the third high flow on the flume, there was a single-thread channel with small a channel bar in it. High terraces were on both sides.

Figure 11. The channel planform evolution during a sequence of floods (flume test 4). The planform evolved through channel incision and the formation of terraces along banks. The terraces were eroded by following floods, during which channel bars were formed. Everything happened cyclically with a duration of 22 minutes.

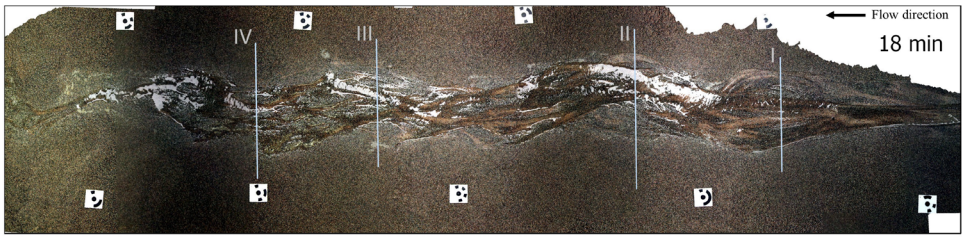

Low flow: Braided channel, channel bars through the whole river and terraces on both sides.

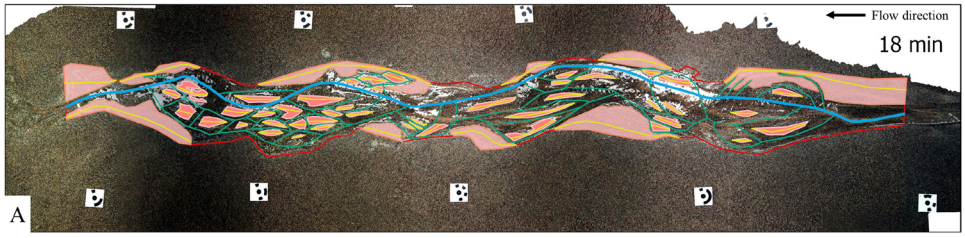

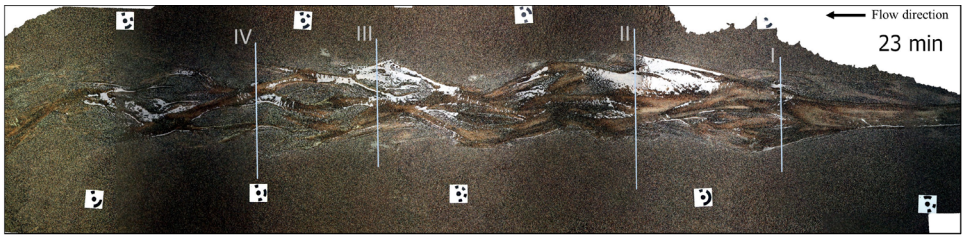

After flood: channel bars are bigger, side channels through the whole channel.

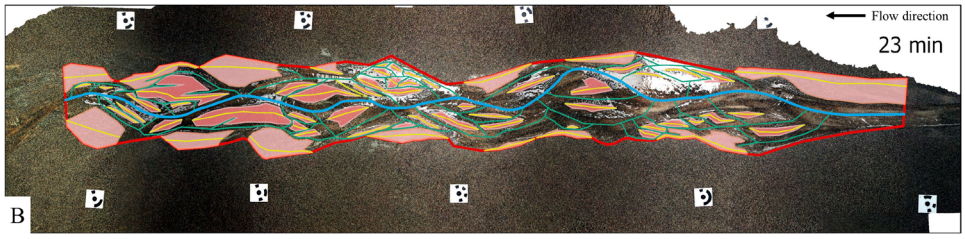

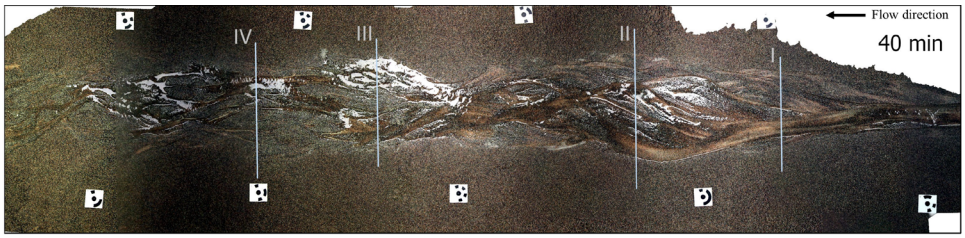

Low flow: Sinuous planform with terraces on the right side and cut banks on the left side.

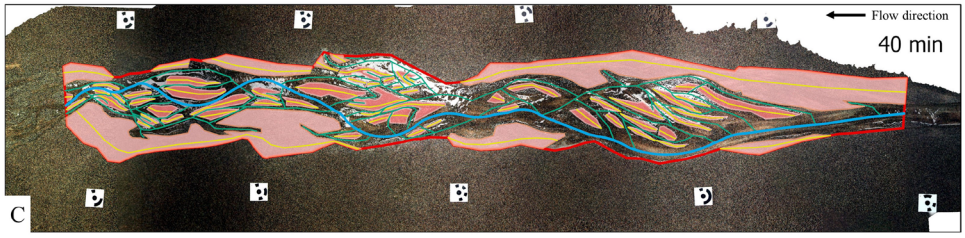

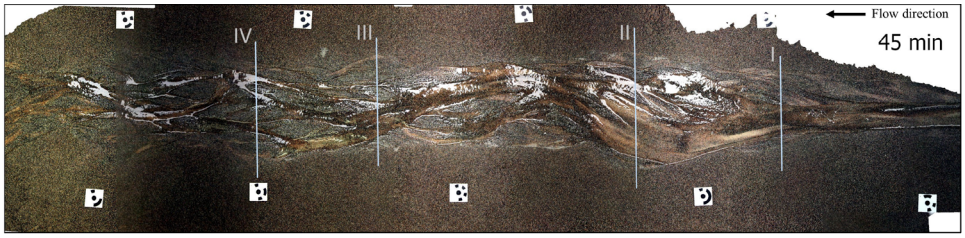

Flood: Higher river sinuosity, inundation of terraces, and active side channels.

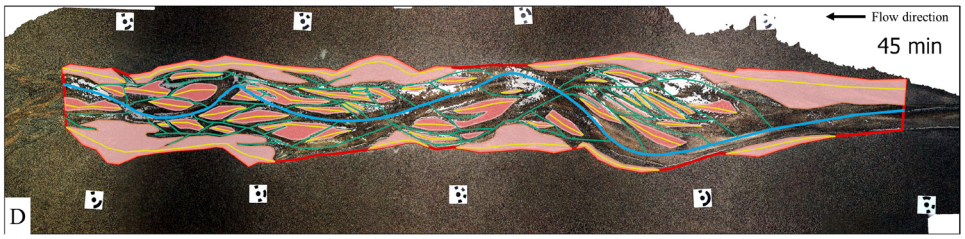

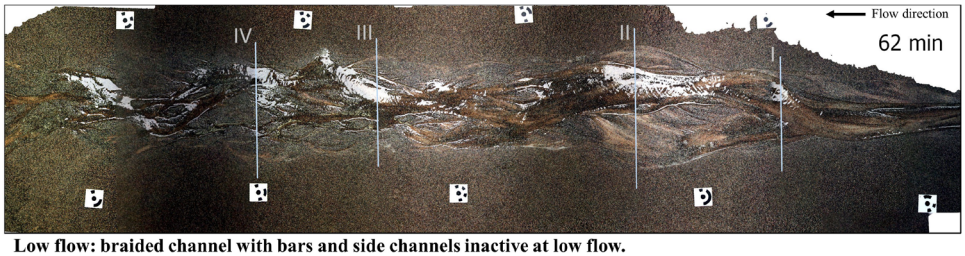

Low flow: braided channel with bars and side channels inactive at low flow.

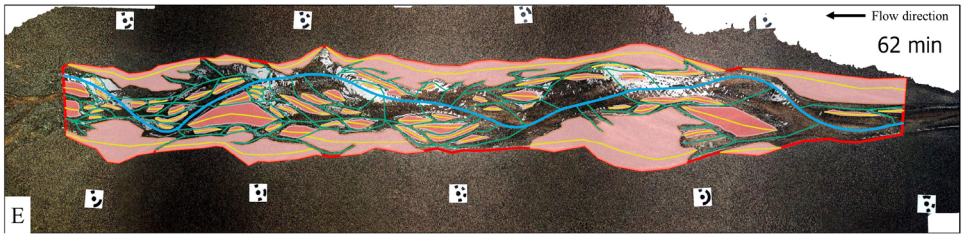

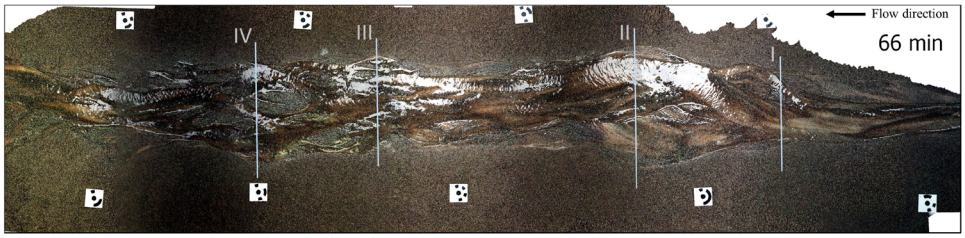

Flood: Wider channel with the inundation of terraces and channel bars.

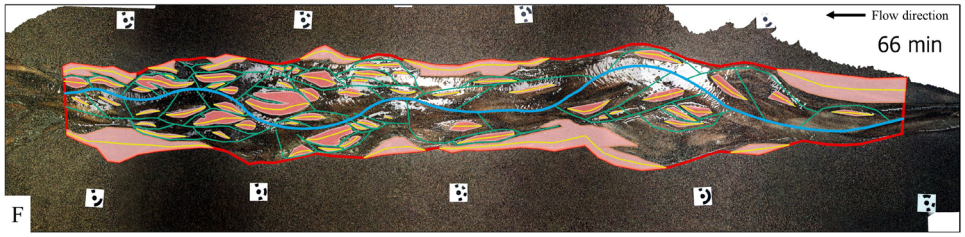

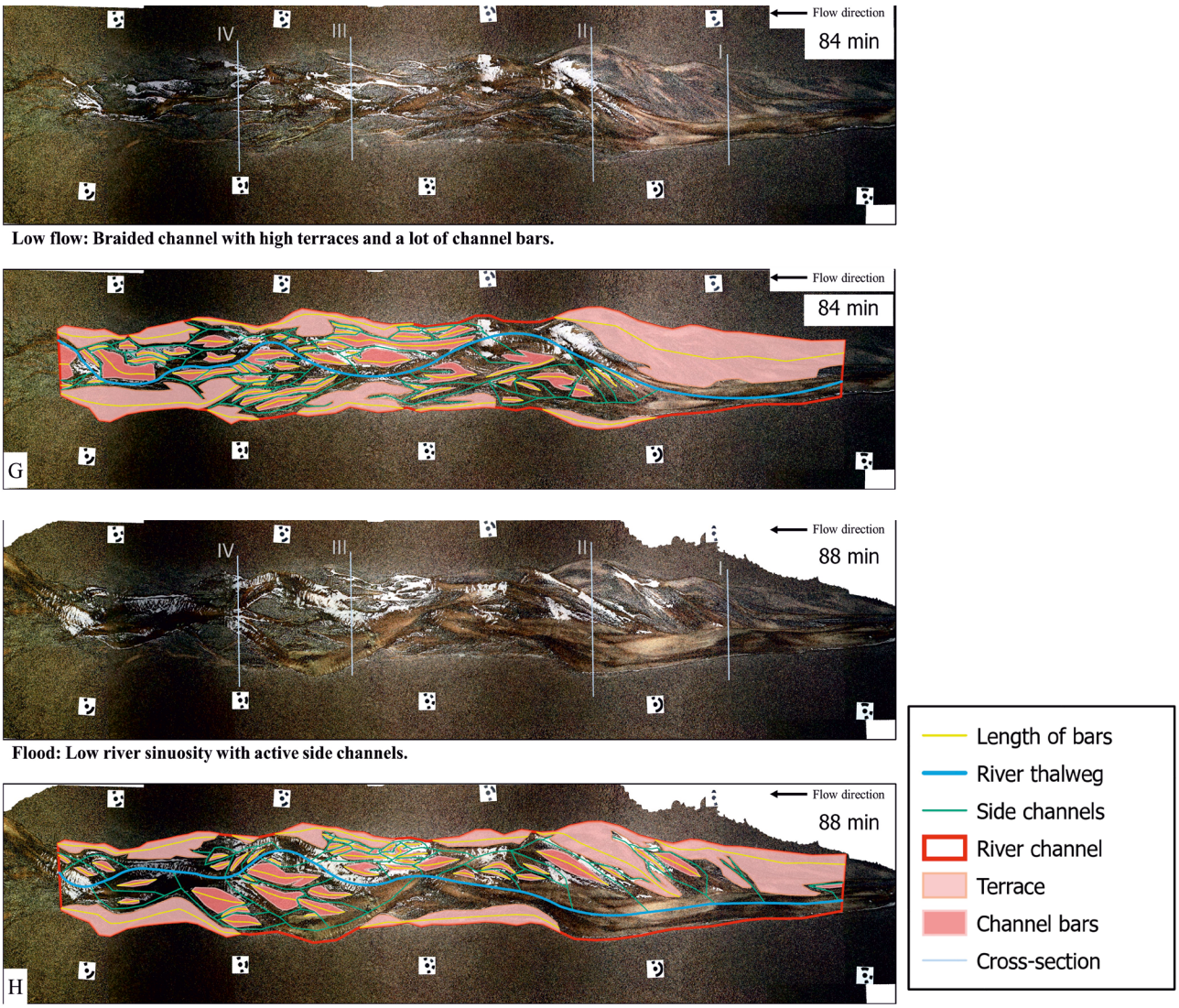

There was a single-thread channel during the flood (66 min) too, though it was wider than the former one. Terraces were on both sides here too. Some reflection from the water disturbed graphs.

From the fourth flood, the third cross-section was analyzed (see Figure 11 for cross-section location). Due to low discharge, slope and the distance from the source, the water here was flowing slowly with a shallow channel and terraces on both sides. A side channel was on the right side with small bars in it. A wider bar was separating the main channel from the second one. When the discharge was increased, the situation changed. The main channel was on the left, while channel bars and active side channels were on the right side of the river.

Figure 12. Cross-sections showing channel planform evolution during flume experiment 4.
Check Figure 11 for the location of cross-sections. 1 (II) - second cross-section from first cycle of flood; (2) IV - fourth cross-section from second cycle of flood;3 (II) - second cross-section from third cycle of flood; (4) III - third cross-section from fourth cycle of flood.
Ch: Channel; T: Terrace; B: Bar; R: Reflection; SCh: Side Channel

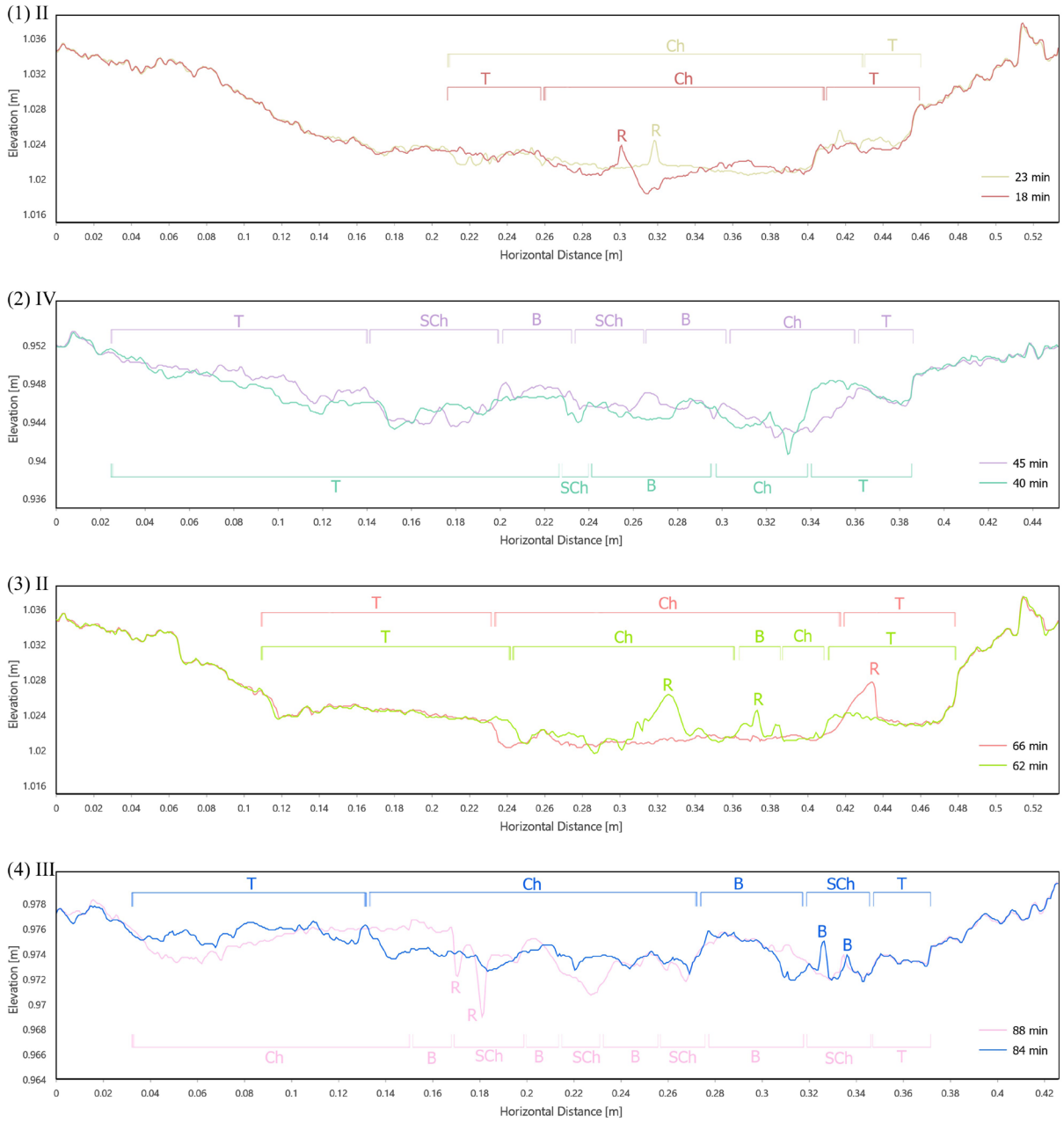

Figure 13. Cross-sections showing the evolution of the channel planform during flume experiment 4. Check Figure 11 for the location of cross-sections

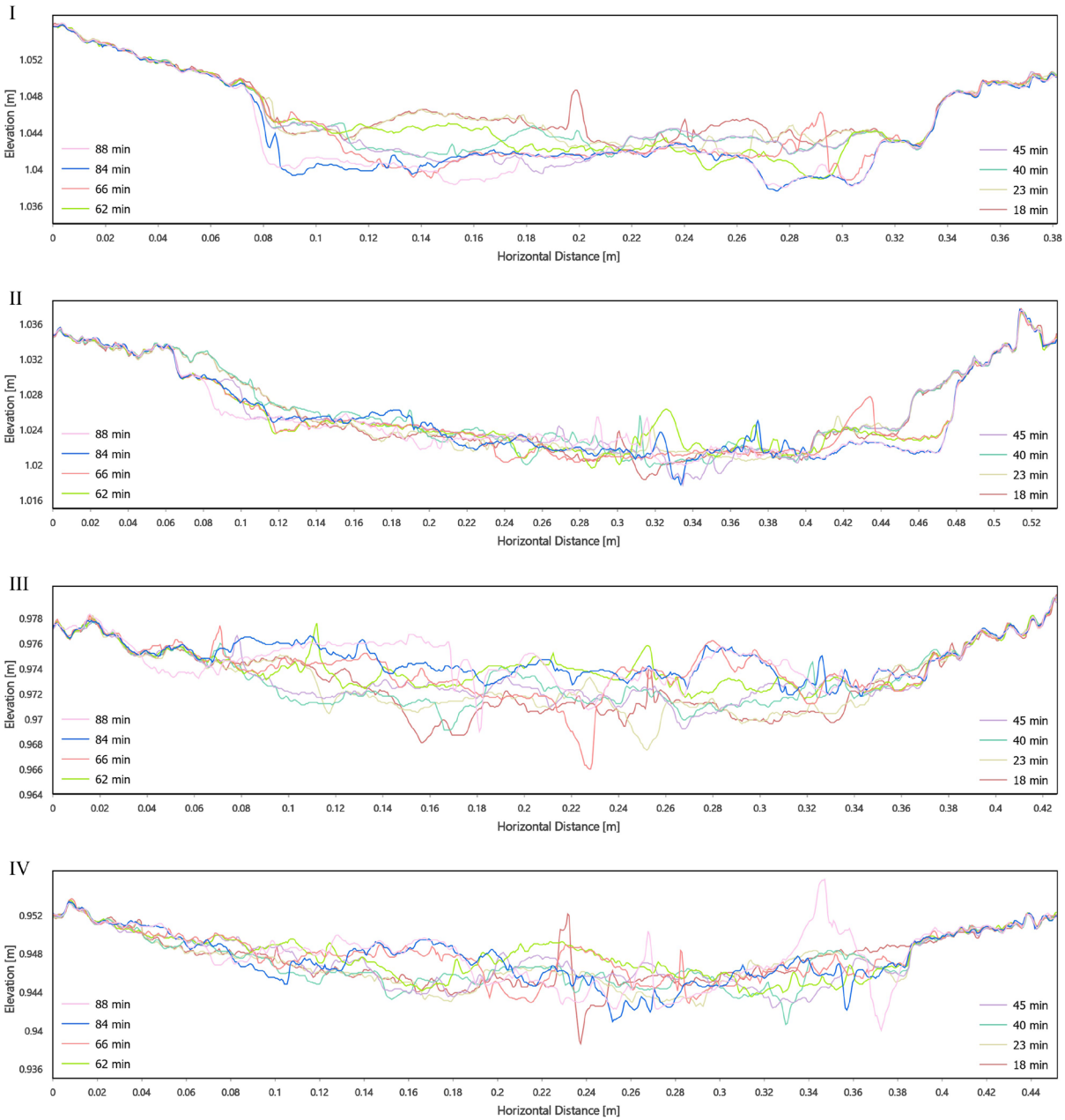

Table 2. Calculations of flume experiments. L_s: thalweg length; L_k: length of channel centerline; V: channel length; H: the line that connects inflection points of the thalweg; ∑ L: total length of the channels; L_b: length of bars and islands.

Flume Test	Minute	L_s	L_k	V	H	∑ L	Whole Channel Area	Area of Bars and Islands	L_b	Number of Bars and Islands	Sinuosity (Leopold and Wolman; Rust)	Braiding Parameter (Rust)	(Area of Bars and Islands / Channel Area) Ratio
1	60	3.6015	2.9276	2.8883	2.9009	18.9438	0.9998	0.4126	11.7983	46	1.2469	4.0849	41.2671
1	120	3.5104	2.9523	2.8896	2.9718	23.5600	1.0959	0.4272	13.6798	64	1.2148	4.7342	38.9812
2	28	2.9370	2.7317	2.7144	2.8490	14.4021	0.8510	0.3185	8.5599	48	1.0820	3.1535	37.4239
2	58	2.9463	2.7324	2.7151	2.7705	12.3226	0.8805	0.5085	9.1012	51	1.0851	3.3520	57.7478
2	88	2.8403	2.7280	2.7150	2.7847	12.4996	0.9140	0.4934	9.5984	40	1.0462	3.5353	53.9772
3	28	3.1313	3.0107	2.9875	3.0054	12.9116	0.9305	0.3349	7.8138	30	1.0481	2.6155	35.9903
3	58	3.3144	3.0138	3.0008	3.1061	14.5632	1.0972	0.3558	8.7986	40	1.1045	2.9321	32.4271
3	88	3.4975	3.0091	3.0011	3.1137	16.4598	1.2567	0.4648	8.7852	37	1.1654	2.9274	36.9856
4	18	2.9280	2.8349	2.8113	2.8416	12.7848	0.6263	0.2359	7.1689	54	1.0415	2.5500	37.6719
4	23	2.9492	2.8194	2.8048	2.8215	14.0042	0.7068	0.2307	8.6070	60	1.0515	3.0686	32.6327
4	40	2.9885	2.8184	2.8062	2.8918	14.4641	0.7686	0.3442	9.5338	62	1.0650	3.3974	44.7835
4	45	3.0182	2.8230	2.8066	2.9035	14.9387	0.7998	0.3108	9.7433	48	1.0754	3.4715	38.8548
4	62	3.0221	2.8131	2.8057	2.9229	17.2742	0.8374	0.3571	10.1246	70	1.0771	3.6085	42.6428
4	66	2.9721	2.8123	2.8047	2.8501	15.5914	0.8496	0.2170	8.6165	66	1.0597	3.0721	25.5427
4	84	3.0028	2.8178	2.8071	2.8789	15.2142	0.8567	0.3973	10.1915	61	1.0697	3.6305	46.3752
4	88	2.9143	2.8132	2.8068	2.8503	13.4766	0.8708	0.3061	8.5176	50	1.0383	3.0347	35.1439

CONCLUSIONS

Our experiments allowed the simulation of processes that potentially occur along the lower Drava River due to prognosticated hydrological and morphological consequences of climatic changes. Climate change is expected to have a significant impact on the physical environment of the lower Drava River. The following changes for the Drava catchment can be confirmed based on the reviewed literature (Formayer et al., 2001; Lóczy, 2019): (i) a significant rise in mean annual temperature, less pronounced in maximum monthly temperature in mountain environments; (ii) increased precipitation totals in the headwaters, (iii) reduced precipitation totals in the lowlands; (iv) increased cloud cover in summer, but in winter, it only increased at higher elevations and decreased in valleys.

Flume tests were performed to investigate the influence of constant discharge, flow reduction, flow enhancement, and a series of floods on channel planform evolution.

From our first flume experiment, we observed the formation of alternate bars that subsequently merged into bigger bedforms and the formation of alluvial islands with a main channel. From some previous studies, the main channel was missing, because they used a steady outflow and sediment feed, causing waterways near the alluvial islands to enlarge, whereas we used a constant discharge,

but without sediment feed. Despite the merging of channel bars and the formation of alluvial islands, we realized the migration of these bedforms.

In the Drava River, although natural fluctuation shows marked seasonal differences, the regulated discharge is more balanced due to river regulation and dams and flow-regulation structures upstream. Furthermore, the river will stay on the same channel with relatively constant channel bars, point bars, alternate bars and alluvial islands.

Due to discharge reduction in flume test 2, the modeled flow was unable to rework and transport sediment from the floodplain. It progressed from a wide channel belt composed of several channels to a single-thread flow with the evidence of dormant channels remaining in the floodplain. Together with other secondary channels, it formed a typical anabranching planform.

On this occasion, the river with less and less discharge would be more concentrated in a single-thread flow and in some places would create an anabranching planform, provided it remains unregulated. Terraces would be present on both sides at higher elevation, and side channels only as dormant channels, although during high flow they could be reactivated. High terraces, alluvial islands and other bedforms can become active again, i.e., inundated during floods.

In our third flume test, when discharge was increased, our studies showed enhanced erosion and the reworking of channel banks, similar to Li et al. (2019) laboratory tests, although, unlike us, they also increased slope. The increase of discharge on the channel resulted in a transition from a meandering to a sinuous planform with more channel bars. On the right side of the river a high bluff zone was formed, which actively developed and eroded.

The floodplain of the lower Drava River is surrounded by flood protection dikes and levees. This situation limited the meanders and sinuosity potential of the river. However, erosion, the reworking of channel banks, and higher risks of high bluffs can still happen on the lower Drava River. The downstream availability of sediments is limited because transported material is retained at all 22 dams of the Drava River. However, during increased flow events, sediments are removed from the channel, and erosion widens the channel, leaving behind bluffs of relatively low height.

Flood series influence anabranching planform development with meandering anabranches (Słowik, 2018; Słowik et al., 2021). In our fourth experiment, the formation and coalescence of channel bars were observed in side channels, while scour channels within the alluvial islands, triggered by alternating flows, developed. Series of floods result in bed incision and the development of channel bars. As the main river continues to incise, the bars unite and produce alluvial islands. High flows activate side channels, and if the incision of a channel prevents this activation, the channel becomes part of the floodplain. The same evolution happens to our study river, which has been changed by dam projects, resulting in reduced bed load conveyance. Dams, which alter sediment loads and outflow, typically result in channel narrowing and degradation below the dam (Petts, 1979; Williams & Wolman, 1984; Collier et al., 2000; Schumm, 2007). In this river flow, certain steps are being taken to restore side channel activity and groundwater supplies (Lóczy et al., 2014; Słowik et al., 2021). However, the availability of sediment and water resources in river basins is critical to the success of these endeavors.

The channel planform alterations produced in the fourth flume experiment are similar to those found in a real river course on the lower Drava River (cf. Słowik et al., 2018). Dam building and previous human-caused modifications (channel straightening, sediment mining, etc.) influenced the river (Słowik et al., 2018; Lóczy, 2019). These circumstances led to the formation of channel bars and bed incision, which are comparable to the processes that occurred when the riverbed of the Drava River was straightened in the 1700s and 1800s. The planform then evolved as a result of the ongoing incision of the main channels, the construction of alluvial islands with scour channels generated by floods, and side channels active at high flows, comparable to the lower Drava (cf, Słowik et al., 2018).

Several features of the evolution of the real lower Drava River course are preserved in the experimental results. The constant discharge flume test shows the merging and migration of bedforms and higher river sinuosity. While the first two can happen on the lower Drava River, its sinuosity cannot be increased because of river regulation. Because of flood protection dikes, the lower Drava River already has a single-thread planform, and in cases of flow reduction (flume test 2), it will have the remains of inactive channels. These would be separated from the main channel with alluvial islands, which will be strengthened over time. The sinuosity ratio from flume test 3 has more difficulties to change in high scale, because of flood protection levees. However, erosion, the reworking of channel banks, and higher risks of high bluffs can still happen on the lower Drava River. The simulation of a series of floods on the last flume experiment generated the construction of an anabranching planform, which correlates with the past floods on the lower Drava River.

REFERENCES

Balatonyi L., Lengyel B., & Berger Á. (2022). Nature-based solutions as water management measures in Hungary. *Modern Geográfia*, *17*(1), 73–85. https://doi.org/10.15170/MG.2022.17.01.05

Bali, L., & Kőkuti, T. (2008). Einige Aspekte Der Untersuchung, der die Kroatisch–Ungarischen Grenze übersteigenden Zusammenarbeit. *Modern Geográfia*, *3*(3), 19–34. http://www.modern-geografia.eu/wp-content/uploads/2012/02/bali_kokuti_2008_3.pdf

Baumgartner, A., Reichel, E., & Weber, G. (1983). *Der Wasserhaushalt der Alpen: Niederschlag, Verdunstung, Abfluß und Gletscherspende im Gesamtgebiet der Alpen im Jahresdurchschnitt für die Normalperiode 1931–1960.* Oldenbourg Verlag.

Berényi A., Pongrácz R. & Bartholy J. (2021). Csapadékszélsőségek változása Európa déli alföldi régióiban az 1951–2019 időszakban. *Modern Geográfia*, *16*(4), 85–101. https://doi.org/10.15170/MG.2021.16.04.05

Blöschl, G., Viglione, A., Merz, R., Parajka, J., Salinas, J. L., & Schöner, W. (2011). *Auswirkungen des Klimawandels auf Hochwasser und Niederwasser.* Österr Wasser- und Abfallw, 63, 21–30. https://doi.org/10.1007/s00506-010-0269-z

Braudrick, C. A., Dietrich, W. E., Leverich, G. T., & Sklar, L. S. (2009). Experimental evidence for the conditions necessary to sustain meandering in coarse-bedded rivers. *Proceedings of the National Academy of Sciences USA* 106:16936–16941. https://doi.org/10.1073/pnas.0909417106

Carrivick, J. L., Smith, M. W., & Quincey, D. J. (2016). Structure from Motion in the geosciences. *Wiley Blackwell*. https://doi.org/10.1002/9781118895818

Cindrić, K., Gajić-Čapka, M., & Zaninović, K. (2009). Observed climate changes in Croatia. In: *Fifth National Communication of the Republic of Croatia under the United Nation Framework Convention on the Climate Change (UNFCCC).* Meteorological and Hydrological Service of Croatia (DHMZ). http://klima.hr/razno/publikacije/climate_change.pdf

Collier, M., Webb, R. H., & Schmidt, J. C. (2000). *Dams and Rivers. A Primer on the Downstream Effects of Dams.* U.S. Geological Survey Circular No. 1126.

Debnath, J., Ahmed, I., & Pan, N. Das. (2015). Impact of anthropogenic activities on channel characteristics : a case study of Muhuri River, Tripura, North-East India. *Archives of Applied Science Research, 7*(7), 27–36.

Eitzinger, J., Daneu, V., Bodner, G., Kubu, G., Loiskandl, W., Macaigne, P., Thaler, S., Schaumberger, A., Wittmann, C., Weidle, F., Kann, A., Murer, E., Krammer, C., Trnka, M., & Hayes, M. (2016). *Drought monitoring system for Austrian agriculture – AgroDroughtAustria* (Final Scientific Report of project "AgroDroughtAustria" of the Austrian Climate Change Research Program). BOKU-Met Report 25. https://meteo.boku.ac.at/report/

Formayer, H., Clementschitsch, L., & Kromp-Kolb, H. (2008). *Regionale Klimaänderungen in Österreich.* Universität für Bodenkultur (BOKU). http://www.wau.boku.ac.at/met.html

Formayer, H., Weber, A., Volk, F., Eckhardt, S., Kromp-Kolb, H., & Boxberger, J. (2001). *Ermittlung der verfügbaren Feldarbeitstage für die Landwirtschaft in Österreich*. Endbericht des Forschungsprojektes Nr. 1086 des BMLF.

Forster, J. E. (1971). *History and description of the Mississippi Basin Model.* MRM Report 1–6. 115–126.

Gobiet, A. (2010). Klimamodelle und Klimaszenarien für Österreich. In R. Hohenauer (Hrsg.), *Auswirkungen des Klimawandels auf Hydrologie und Wasserwirtschaft in Österreich – Präsentation aktueller Studien (*pp. 11–24). Österreichischer Wasser- und Abfallwirtschaftsverband.

Goler, R. A., Frey, S., Formayer, H., & Holzmann, H. (2016). Influence of climate change on river discharge in Austria. *Meteorologische Zeitschrift, 25*(5), 621–626. https://doi.org/10.1127/metz/2016/0562

Holzmann, H., Lehmann, T., Formayer, H., & Haas, P. (2010). Auswirkungen möglicher Klimaänderungen auf Hochwasser und Wasserhaushaltskomponenten ausgewählter Einzugsgebiete in Österreich. *Österr Wasser- und Abfallw, 62*(1–2), 7–14. https://doi.org/10.1007/s00506-009-0154-9

Iskriva, Z. (n.d.). Drava in Hungary: Description of the pilot site. *Sustainable Integrated Management of International River Corridors in SEE Countries.* http://www.see-river.net/drava-hungary.2.html

Kiss, K. (2021). *Investigation of channel pattern evolution of experimental rivers.* [Doctoral dissertation, University of Pécs].

Kiss, T., Andrási, G., & Hernesz, P. (2011). Morphological alternation of the Drava as the result of human impact. *AGD Landscape and Environment, 5*(2), 58–75.

Kleinhans, M. G. (2010). Sorting out river channel patterns. *Progress in Physical Geography, 34*(3), 287–326. https://doi.org/10.1177/0309133310365300

Kleinhans, M. G., Dijk, W. M., Lageweg, W. V., Hoyal, D. C., Markies, H., Maarseveen, M. V., Roosendaal, C., Weesep, W. V., Breemen, D. V., Hoendervoogt, R., & Cheshier, N. R. (2014). Quantifiable effectiveness of experimental scaling of river- and delta morphodynamics and stratigraphy. *Earth-Science Reviews, 133*, 43–61.

Kromp-Kolb, H., & Schwarzl, I. (Hrsg.) (2009). *Anpassung an den Klimawandel in Österreich [Adaptation to climate change in Austria].* Umweltbundesamt.

Leopold, L. B., & Wolman, M. G. (1957). River channel patterns: Braided, meandering and straight. *U.S. Geological Survey, Professional Paper, 282*(B), 1–85. https://doi.org/10.3133/pp282B

Lóczy, D. (2019). *The Drava River.* https://doi.org/10.1007/978-3-319-92816-6

Lovász, G., (1972). *A Dráva–Mura-vízrendszer vízjárási és folyási viszonyai.* Akadémiai Kiadó.

Lovász, G., (1983). *Surface runoff of the Drava-Mura drainage system.* Geographical Research Institute, Hungarian Academy of Sciences.

Lovász, Gy. (1972). *A Dráva-Mura vízrendszer vízjárási és lefolyási viszonyai.* Akadémiai Kiadó,

Lowe, D. G. (2004). Distinctive Image Features from Scale-Invariant Keypoints. *International Journal of Computer Vision*, *60*(2), 91–110. http://dx.doi.org/10.1023/B:VISI.0000029664.99615.94

Matulla, C., Groll, N., Kromp-Kolb, H., Scheifinger, H., Lexer, M. J., & Widmann, M. (2002). Climate change scenarios at Austrian National Forest Inventory sites. *Climate Research, 22*(2), 161–173. https://doi.org/10.3354/cr022161

Métivier, F., Lajeunesse, E., & Devauchelle, O. (2016). Laboratory rivers: Lacey's law, threshold theory, and channel stability. *Earth Surface Dynamics, European Geosciences Union, 5*, 187–198. https://doi.org/10.5194/esurf-2016-47

Peakall, J., Ashworth, P. J., & Best, J. L. (1996). Physical modelling in fluvial geomorphology: principles, applications and unresolved Issues. In Rhoads B., & Thorn C. (Eds.), *The scientific nature of geomorphology edition: proceedings of the 27th Binghamton symposium* (pp. 221–252). Wiley.

Petts, G. E. (1979). Complex response of river channel morphology subsequent to reservoir construction. *Progress in Physical Geography: Earth and Environment*, *3*(3), 329–362. https://doi.org/10.1177/030913337900300302

Pirkhoffer, E., Halmai, Á., Czigány, S., Bugya, T., Rábay, A., Bötkös, T., Nagy, G., Balassa, B., Jancskárné Anweiler, I., & Lóczy, D. (2014). New opportunities for experiments in fluvial geomorphology: The flume PTETHYS. *Hungarian Geographical Bulletin*, *63*(4), 425–436. https://doi.org/10.15201/hungeobull.63.4.4

Prettenthaler, F. (2007). *Wasser & Wirtschaft im Klimawandel: Konkrete Ergebnisse am Beispiel der sensiblen Region Oststeiermark.* Verlag Der Österreichischen Akademie Der Wissenschaften.

Rickenmann, D. (Hrsg.) (2009). *Extremereignisse: Ereignisbezogene Dokumentation-Prozesse Bergstürze, Hochwasser, Muren, Rutschungen und Lawinen*. Institute für Alpine Naturgefahren und Forstliches Ingeneurwesen, Universität für Bodenkultur (BOKU).

Ristić, R., Ljujić, M., Despotović, J., Aleksić, V., Radić, B., Nikić, Z., Milćanović V., Malušević I., & Radonjić, J. (2013). Reservoir sedimentation and hydrological effects of land use changes-case study of the experimental Dićina river watershed. *Carpathian Journal of Earth and Environmental Sciences, 8*(1), 91–98.

Rust, B. R. (1978). A classification of alluvial channel systems. In A. D. Miall (Ed.), *Fluvial sedimentology* (pp. 187–198). Canadian Society of Petroleum Geologists.

Schmidli, J., Schmutz, C., Frei, C., Wanner, C., & Schär, C. (2002). Mesoscale precipitation in the Alps during the 20th century. *International Journal of Climatology, 22,* 1049–1074.

Schöner, W., Böhm, R., & Haslinger, K. (2011). Klimaänderung in Österreich – hydrologisch relevante Klimaelemente. *Oesterr Wasser Abfallwirtsch, 1–2,* 11–20.

Schumm, S. A. (2007). *River variability and complexity*. Cambridge University Press. https://doi.org/10.1017/CBO9781139165440

Schumm, S. A., & Khan, H. R. (1971). Experimental study of channel patterns. *Nature, 233*, 407–409.

Schumm, S. A., & Khan, H. R. (1972). Experimental study of channel patterns. *GSA Bull*, *83*(6), 1755–1770. https://doi.org/10.1130/0016-7606(1972)83[1755:ESOCP]2.0.CO;2

Słowik, M. (2018). The formation of an anabranching planform in a sandy floodplain by increased flows and sediment load. *Earth Surface Processes and Landforms, 43*(3), 623–638. https://doi.org/10.1002/esp.4272

Słowik, M., Kiss, K., Czigány, S., Gradwohl-Valkay, A., Dezső, J., Halmai, Á., Marciniak, A., Tritt, R., & Pirkhoffer, E. (2021). The influence of changes in flow regime caused by dam closure on channel planform evolution: insights from flume experiments. *Environmental Earth Sciences*, *80*(4), 1–18. https://doi.org/10.1007/s12665-021-09437-5

Smiatek, G., Kunstmann, H., Knoche, R., & Marx, A. (2009). Precipitation and temperature statistics in high-resolution regional climate models: evaluation for the European Alps. *Journal of Geophysical Research, 114*(19), 1–16. https://doi.org/10.1029/2008JD011353

Smith, M. W., Carrivick, J. L., & Quincey, D. J. (2016). Structure from motion photogrammetry in physical geography. *Progress in Physical Geography: Earth and Environment*, *40*(2), 247–275. https://doi.org/10.1177%2F0309133315615805

South-Transdanubia Water Management Directorate. (n.d.). Retrieved November 17, 2021, from http://ddvizig.hu/en/

Strauss, F., Formayer, H., & Schmid, E. (2013). High resolution climate data for Austria in the period 2008–2040 from a statistical climate change model. *Int J Climatol, 33*(2), 430–443.

Struiksma, N., Olesen, K. W., Flokstra, C., & De Vriend, J. H. (1985). Bed deformation in curved alluvial channels. *Journal of Hydraulic Research*, *23*(1), 57–79. https://doi.org/10.1080/00221688509499377

Tal, M., & Paola, C. (2007). Dynamic single-thread channels maintained by the interaction of flow and vegetation. *Geology, 35,* 347–350. https://doi.org/10.1130/G23260A.1

Tiffany, J. B., & Nelson, G. A., (1939). Studies of meandering of model-streams. *Transctions. American Geophysical Union, 20*(4), 644–649. https://doi.org/10.1029/TR020i004p00644

van Dijk, W. M., van de Lageweg, W. I., & Kleinhans, M. G. (2012). Experimental meandering river with chute cutoffs. *Journal of Geophysical Research, 117*(3), https://doi.org/10.1029/2011JF002314

van Dijk, W. M., van de Lageweg, W. I., & Kleinhans, M. G. (2013). Formation of a cohesive floodplain in a dynamic experimental meandering river. *Earth Surface Processes and Landforms 38, 1550–1565.* https://doi.org/10.1002/esp.3400

Williams, G. P. & Wolman, M. G. (1984). Downstream Effects of Dams on Alluvial Rivers. U.S. *Geological Survey Professional Paper No. 1286.*

Zhiwei Li, Z. Li, Xinyu Wu, X. Wu, Peng Gao, P. Gao. Li, Z., Xinyu, W., & Gao, P. (2019). Experimental study on the process of neck cutoff and channel adjustment in a highly sinuous meander under constant discharges. *Geomorphology, 327*, 215–229. https://doi.org/10.1016/j.geomorph.2018.11.002

Zolezzi, G., Guala, M., Termini, D., & Seminara, G. (2005). Experimental observations of upstream over deepening. *Journal of Fluid Mechanics, 531*, 191–219. https://doi.org/10.1017/S0022112005003927